Macrosegregation Prediction for DC Casting of Ternary Bronze Alloys

J. Hao, M. Grasser, A. Ishmurzin, M. Wu, A. Ludwig

Christian-Doppler Laboratory for
Multiphase Modeling of Metallurgical Processes
University of Leoben, Dept. of Metallurgy
A-8700 Leoben, Austria

J. Riedle, R. Eberle

Wieland Werke AG Ulm
Wielandstraße 26

D-89269 Vöhringen, Germany

Keywords: Tin bronzes, thermodynamics, ternary, solidification, casting, macrosegregation

Abstract

The paper discusses simulation results for columnar solidification of ternary bronze alloys in continuous casting of rectangular casting geometries. Thermodynamics of Cu-Sn-P is included by using spline-interpolation techniques to model the liquidus surface and the solubility of Sn and P in the different phases. The applied volume-averaged solidification model considers two interpenetrating continua, i.e. the melt as the primary phase and columnar dendrites as the secondary phase. At the interface it is distinguished explicitly between interface and average concentrations. The formation of columnar dendrites is approximated by growing cylinders. After their formation at the mold/metal interface, they are considered to move continuously with the applied casting speed. The velocity field of the melt flow is obtained by solving the momentum conservation equation and within the mushy zone we consider hydrodynamic interaction between melt and solid and local formation of microsegregation. This solidification model is applied to a laboratory continuous casting process. The simulated liquid and solid concentrations are compared with ternary Scheil calculations and, in addition, the average mixture concentration of the simulation results is validated by experimental concentration measurements.

1 Introduction

Bronzes and especially Phosphor bronzes are among the oldest engineering materials still used for many different applications. The most economical way to produce Phosphor bronze is DC casting. Figure 1 shows a schematic sketch of a vertical DC casting process. A vertical continuous casting machine consists mainly of the mold with a tundish or a melting furnace and the mechanical-hydraulic strand withdrawal mechanism. The melt is kept at casting temperature in the heated tundish from where it flows into the mold. The mold itself holds the melt and in addition extensively

cools it. This leads to the formation of a solidified shell at the beginning and finally to complete solidification of the strand.

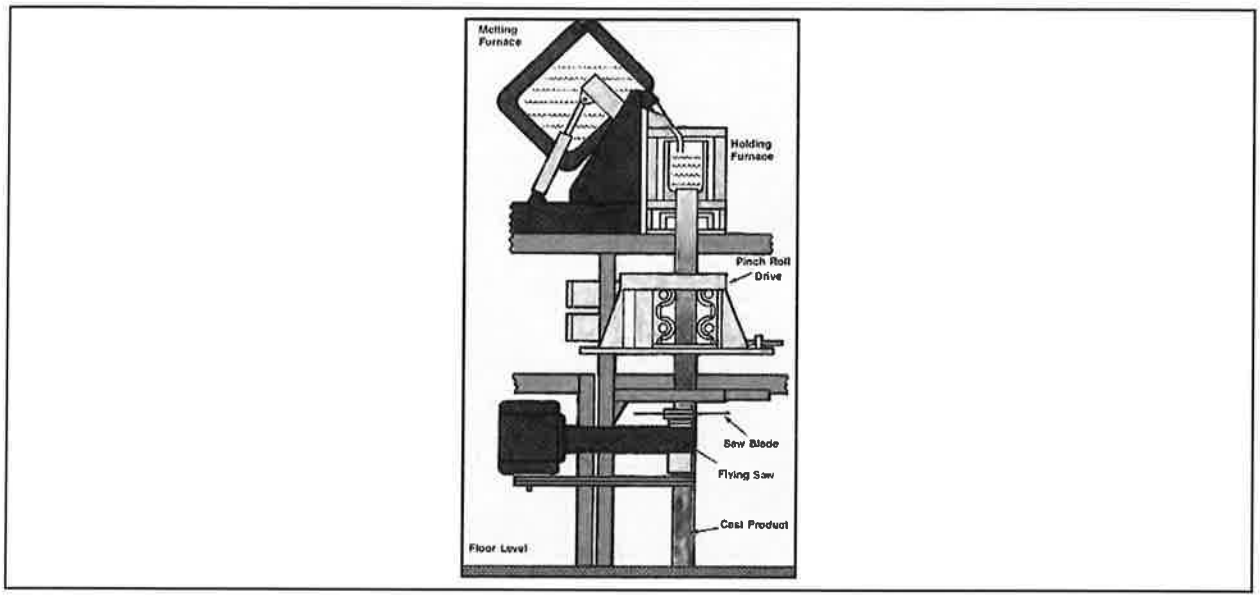

Figure 1: Schematic sketch of a vertical DC caster for bronze [1].

Since bronze is a metallic alloy with a solidification interval of about 200 K, depending on the alloy composition, during casting a region called mushy zone develops where both liquid melt and solidifying dendrites are present. Pronounced segregation takes place in bronzes because of the slow diffusion of Sn in the solid and the wide solidification interval. Figure 2 shows a typical microstructure observed in vertical DC casting of bronze just after casting without any heat treatment. On the left side the phase distribution at an outer boundary is shown whereas on the right the microstructure in the centre of the casting is displayed. The location of both micrographs is indicated schematically in the middle part of Figure 2. It is obvious that the microstructure at the centre is finer with less - eutectoid compared to the outer boundary region. Measurements reveal that tin content at the outer boundary is highest and gradually decreases towards the centre. This concentration inhomogeneity is often referred to as macrosegregation which forms due to microsegregation combined with relative motion between the liquid and the dentrite in the mushy zone. Figure 3 shows such a profile as measured by industry. Since it is not possible to remove this macroscopic concentration inhomogeneity by heat treatment, it is of great importance to reduce its formation directly during casting.

Since the pioneer work of Kaufman and Bernstein in 1970 [2], calculations of phase diagrams have become a widely used tool for predicting thermodynamic information by computational techniques. This method, known as the CALPHAD method (CALculation of PHAse Diagrams) [3, 4], enables the prediction of phase evolution and of corresponding solidification paths by taking into account different cooling rates, back diffusion and/or coarsening [5, 6, 7]. During the last years it was tried to improve the accuracy of macrosegregation prediction in DC casting of non-ferrous alloys by including thermodynamics of higher order systems. For example Eskin [8] discussed the formation of segregation for a ternary Al-alloy based on a two phase model for equiaxed solidification. He stated

that direct coupling between thermodynamic calculations and CFD simulations might be rather time consuming, especially if an industrial size casting process is considered. Besides, improvements were done to numerically describe the formation of macrosegregation in DC casting of bronze [9, 10, 11]. To model such a solidification process conservation equations for mass, enthalpy and solute were considered on the macroscopic scale and thermodynamic equilibrium conditions on the liquid/solid interfacial microscale. Ludwig and co-workers proposed a method [10, 11] to couple thermodynamic data with a multiphase solidification model. Since direct coupling is rather time consuming, the coupling is done by providing access to thermodynamic data through linearization methods, splines or tabulation and interpolation techniques like ISAT (In-Situ Adaptive Tabulation) [12].

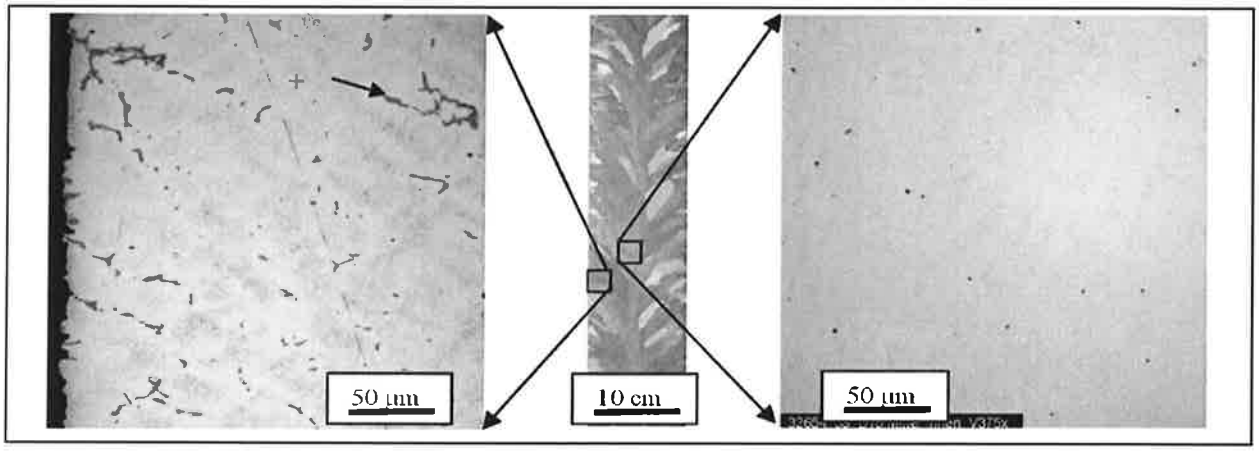

Figure 2: Micrographs taken from a continuous casting strand of CuSn8P0.005 bronze. Left: microstructure at the outer boundary. Dark regions show eutectoid structure where the rigid – eutectoid is present. Middle: columnar grain structure; rectangles: schematic position of the two micrographs left and right. Right: microstructure in the centre, here the microstructure is more homogeneous than at the outer boundary because almost no eutectoid is present [13].

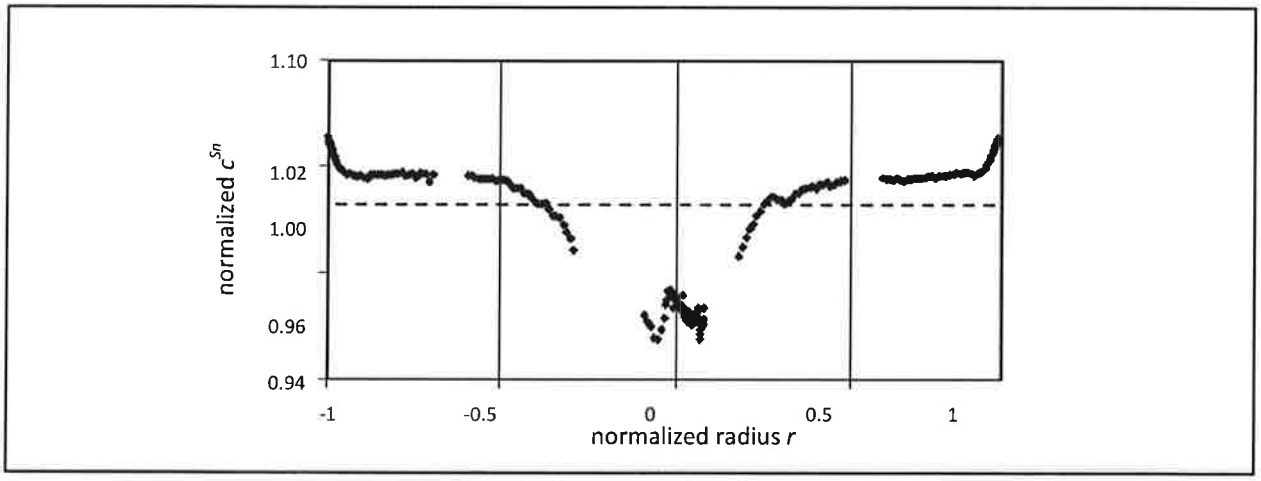

Figure 3: Normalized macrosegregation profile of Sn for a round bloom (CuSn7.6P0.022 alloy). Positive macrosegregation is obtained at the surface and negative one at the center [3].

2 Model Description

During solidification of continuous casting of bronze, equiaxed and/or columnar dendritic growth is observed depending on the applied casting conditions. A multiphase model for columnar and/or equiaxed solidification has been developed by Ludwig, Wu and co-workers from 2002 to 2007 [14-17]. For the simulations discussed in the present paper this model is applied whereas nucleation and growth of equiaxed grains are neglected. Flow phenomena like forced convection, shrinkage induced feeding flow as well as thermo-solutal convection, grain sedimentation or exudation, etc. have an impact on the macrosegregation distribution whereas microsegregation only depends on the thermodynamics of the special system. The thermodynamic information of Cu-Sn-P as published in [10-12] is included by coupling pre-calculated thermodynamic data with the multiphase model. In the recent paper splines of third order are used to model thermodynamics during solidification. Here, as a first attempt for the prediction of macrosegregation, just forced convection and shrinkage induced feeding flow, modelled by taking into account the density difference between liquid and solid, are applied.

Figure 4 shows the liquidus surface of the Cu rich corner of the ternary phase diagram for Cu-Sn-P (based on calculations with Thermo-Calc) including different monovariant lines. In the calculation with the multiphase solidification code, the liquidus surface T_L and the concentration of the two alloying elements in the solid at the solid/liquid interface $\tilde{c}_c^{Sn}$ and $\tilde{c}_c^{P}$ are based on computational thermodynamics (Thermo-Calc). For the industrial application of the model these three thermodynamic functions are spline-interpolated over the whole area [12]. In general, solidification of bronze alloys starts with the formation of dendrites. The black arrows in Figure 4 show an example of a solidification path (CuSn6P0.5) as proposed by a ternary Scheil calculation. Point A indicates the initial alloy concentration whereas point B marks the end of solidification. During primary solidification the melt enriches and so the solidification path crosses the first peritectic groove at P_1. Between P_1 and the second peritectic groove P_2 the melt forms and between P_2 and the eutectic groove E forms from the melt. In the eutectic groove E two binary eutectics, first + Cu_3P and later + Cu_3P form. As soon as the concentration of the remaining melt fits to a concentration that corresponds to the eutectic groove, the binary eutectics form and the melt concentration follows the eutectic groove until it reaches the ternary eutectic point (B). There the formation of the ternary eutectic + Cu_3P + finally terminates the solidification process. Note that, if back diffusion in the solid phases (, ,) is significant, the solidification path may not reach the ternary eutectic point (B), and that, due to a larger solubility of Sn in and , the solidification path turns at point P_1 towards lower Sn concentrations.

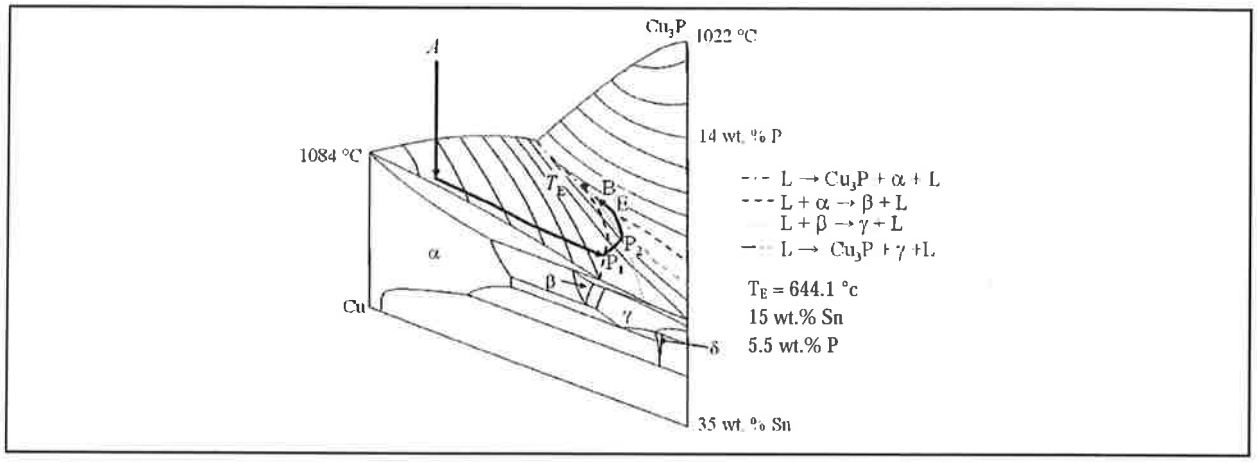

Figure 4: 3D liquidus surface with isotherms for the ternary phase diagram Cu-Sn-P in the Cu rich corner up to 35 wt. % Sn and 14 wt. % P (based on calculations with Thermo-Calc, database CuSnII). Broken lines: monovariant lines of the liquidus surface; front view: binary phase diagram of Cu-Sn; black arrows: solidification path of an alloy with concentration A (CuSn6P0.5) according to the Thermo-Calc Scheil model; P_1: first peritectic groove, P_2: second peritectic groove, E: eutectic groove, B: end of solidification, T_E: ternary eutectic point. The phases labeled in the figures are ~ Cu (max. Sn 15.8 wt. %); ~ $Cu_{17}Sn_3$; ~ Cu_3Sn; ~ $Cu_{41}Sn_{11}$; Cu_3P ~ 14 wt. % P [18].

The here applied thermodynamic model is developed for modelling peritectic transformation in a ternary system whereas a model for eutectic transformation is in development. The concentration of P close to the second peritectic groove (P_2, Figure 4, see also Figure 5) increases rapidly with slightly increasing volume fraction solid. To avoid approaching the first part of the eutectic groove, solidification is stopped at a certain point of liquid concentration. After reaching this point, the mass transfer rate is set to zero and from here on solidification is switched off. However, the suddenly decreasing mass transfer rate from a large value to zero may cause numerical oscillations. To avoid such problems, a continuous function (sigmoid function) is applied in the calculation as following:

$$f(c_l) = \frac{M_{lc}}{1 + e^{(0.004 - d(c_l, c_l^{cr}))}} \quad (1)$$

Here, M_{lc} is the mass transfer rate from liquid to columnar, c_l is the liquid concentration, c_l^{cr} is the critical liquid concentration where mass transfer rate has to be zero, is the parameter for controlling the shape of a sigmoid function and $d(c_l, c_l^{cr})$ is the distance between c_l and c_l^{cr} which is calculated by:

$$d(c_l, c_l^{cr}) = \sqrt{\left(c_l^{Sn} - c_l^{cr,Sn}\right)^2 + \left(c_l^{P} - c_l^{cr,P}\right)^2} \quad (2)$$

Note that the mass transfer rate is reduced by one half as the distance between c_l and c_l^{cr} approaches 0.004. Figure 6 shows sigmoid functions with different values of . It can be seen that the mass transfer rate is reduced to zero smoothly by this function. And it should be noted that a larger value

of can make the function steeper whereas a smaller one leads to a smoother function. The appropriate value for should be chosen to avoid the divergence problems and avert the loss of computational accuracy. In our calculation is set to be 1000 which is reasonable for us.

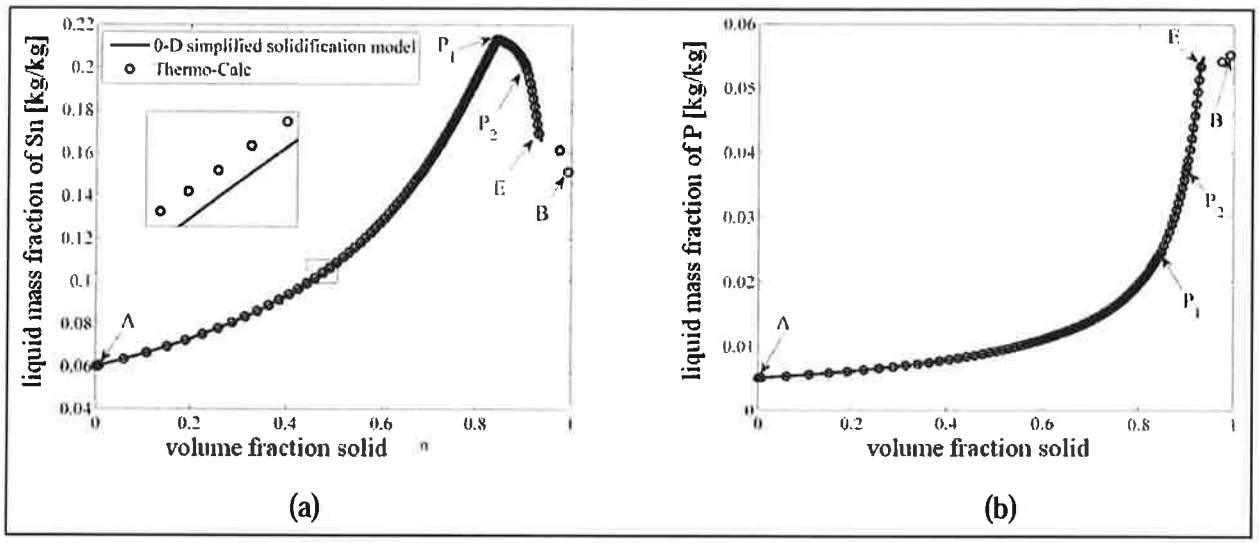

Figure 5: Scheil curves calculated with Thermo-Calc for the alloy CuSn0.58P0.048 for (a) Sn and (b) P. Here c_0 is the initial alloy concentration, P_1 corresponds to the beginning of the first peritectic reaction L + → , P_2 to the beginning of the second peritectic reaction L + → , E to the beginning of the eutectic groove, and B to the end of solidification according to the Thermo-Calc Scheil model [3].

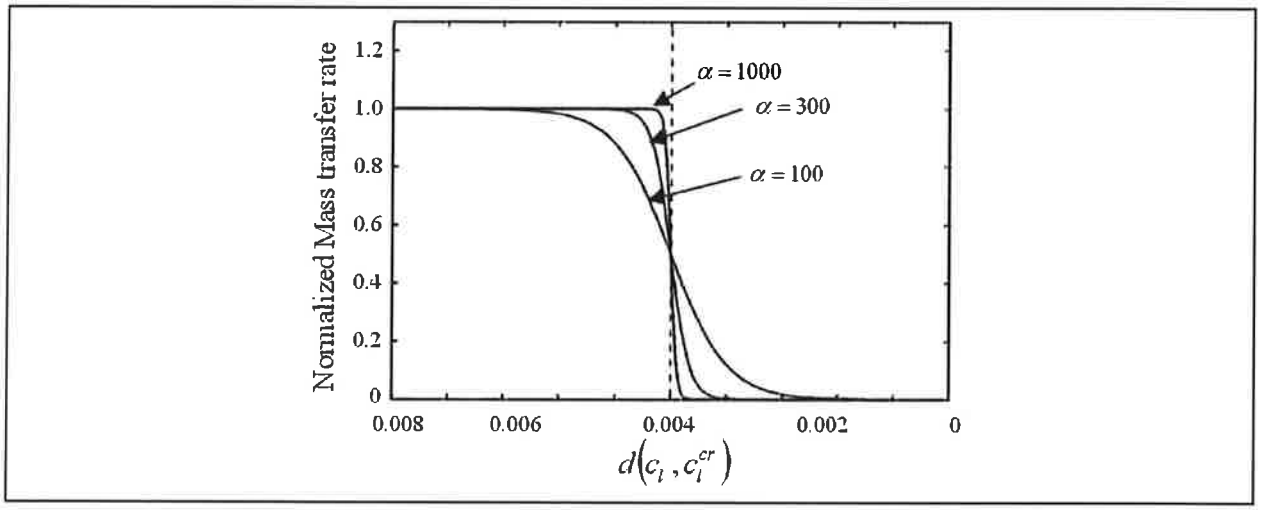

Figure 6: Sigmoid function used to reduce mass transfer rate to zero when liquid concentration c_l reaches critical liquid concentration c_l^{cr}.

3 Geometry and Boundary Conditions

The present model was applied to a laboratory DC casting process as displayed in Figure 7a where ① marks the graphite tundish, ② the position of the inlet in the calculation and ③ the graphite mold. ④ indicates the liquid region, ⑤ the mushy zone and ⑥ the solidified strand. For the process simulation one quarter of the 3D geometry was calculated and therefore two symmetry planes were considered. The simulation was started with hot melt T_{cast} = 1523 K and a casting speed of $\bar{u}_{cast}$ =1.66 mm·s^{-1}. Calculations were done for the ternary alloy CuSn5.8P0.048.

Figure 7b displays the grid and Figure 7c shows the boundary conditions. Here ① indicates the position of the inlet where a pressure inlet is taken. ② marks the upper part of the mold which is assumed to be isolating with a constant temperature T = 1523 K. ③ indicates the second part of the mold which has a linear temperature distribution from 1523 K to 1173 K. ④ shows the third part of the mold where a constant temperature of T = 1173 K is taken and ⑤ assigns a linear temperature distribution from 1173 K to 1087 K. ⑥ indicates the position the first water cooling zone with a heat flux of h = -325,000 W·m^{-2} applied at the mold wall. The following two parts ⑦ and ⑧ have two different heat flux values at the wall which are h = -349,000 W·m^{-2} and h = -186,000 W·m^{-2}. ⑨ shows the position of the outlet where a velocity outlet $\bar{u}_{cast}$ = 1.66 mm·s^{-1} has been considered. The grid size is 1.728 mm^3 in the strand and 125 mm^3 in the mold. The heat transfer coefficient between the strand and the mold is 3000 W·m^{-2}·K^{-1}. Table 1 gives the material data for the simulation including density, heat capacity and heat conductivity. Note that the density difference of liquid and solid is taken into account.

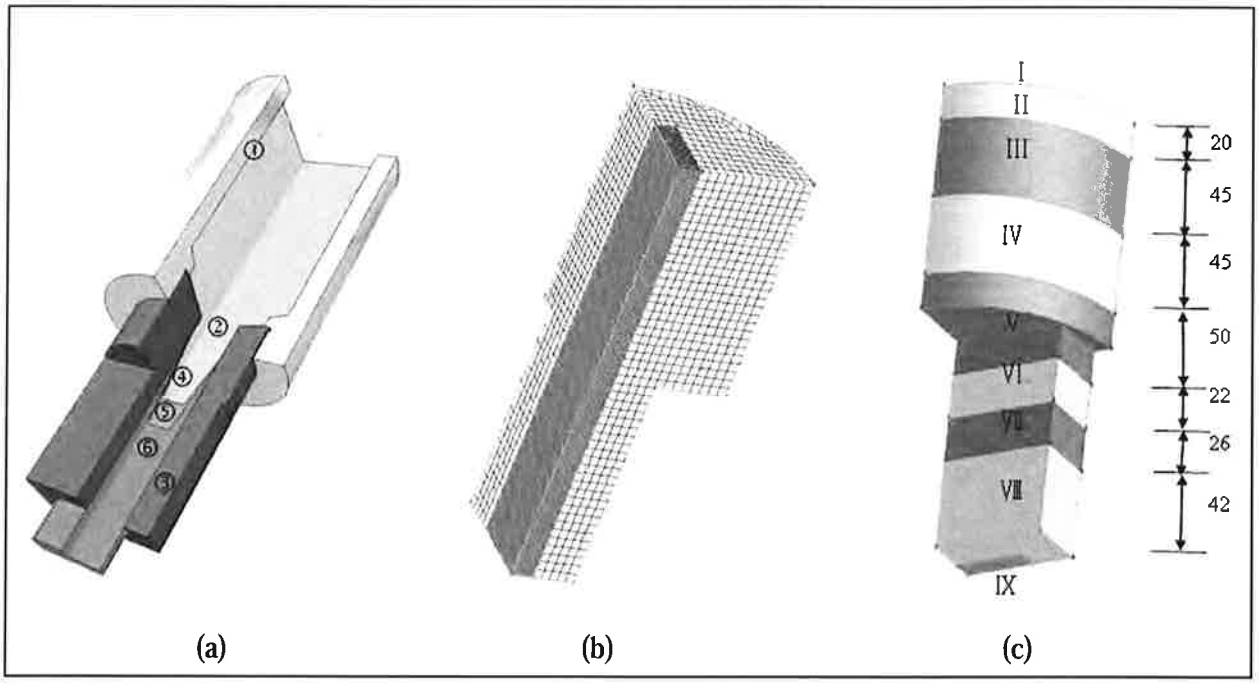

Figure 7: (a) Laboratory geometry. ① marks the graphite tundish, ② the position of the inlet of the calculation and ③ the graphite mold. ④ indicates the liquid region, ⑤ the mushy zone and ⑥ the solidified strand. (b) Grid for calculation. The grid size is 1.728 mm^3 in the strand and 125 mm^3 in the mold. (c) Boundary conditions of the geometry. I marks the position of the inlet, II to VIII indicate different parts of the mold which have different boundary conditions and IX marks the position of the outlet.

Table 1: Material Data List

	Material	Density ($kg \cdot m^{-3}$)	Heat Capacity ($J \cdot kg^{-1} \cdot K^{-1}$)	Thermal Conductivity ($W \cdot m^{-1} \cdot K^{-1}$)
Strand	CuSn5.8P0.048	7810 (liquid) 8565 (solid)	454	96 (liquid) 184 (solid)
Mold	Graphite	1800	2000	60

4 Results and Discussion

The model described above is used to perform solidification simulation with the commercial CFD software FLUENT considering the already mentioned boundary conditions and material data. The obtained steady state results are presented in the following. For discussion the temperature field, the velocity field, the liquid concentrations and the solid concentrations as well as the mixture concentrations are displayed and described.

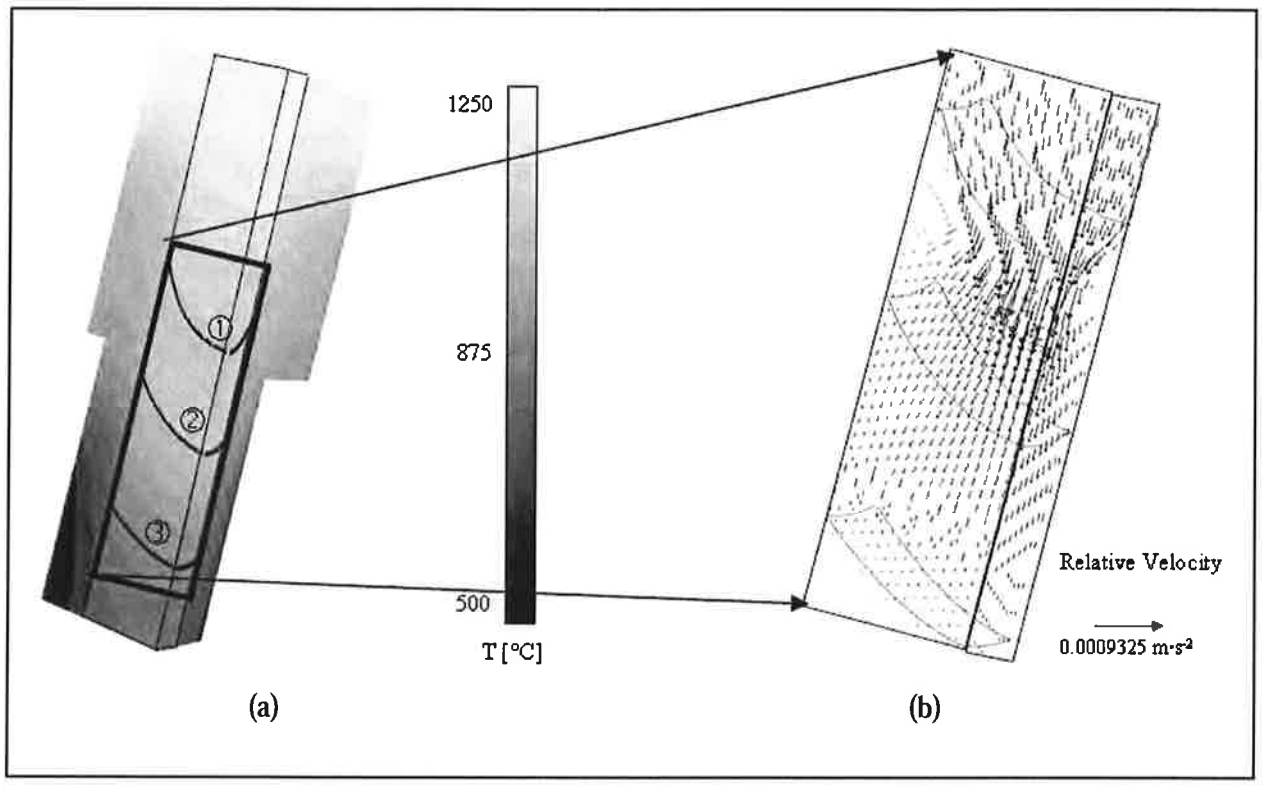

Figure 8: (a) Temperature field in the casting and the mold. Black lines: ① iso-surface of the liquidus temperature of the casted alloy $T_{liquidus}$ = 1259 K, ② the volume fraction solid f_c = 0.5, and ③ the iso-surface of f_c = 0.9. (b) Relative velocity field between liquid and solid at the region marked in (a) with the rectangle.

Figure 8a displays the calculated temperature field at the symmetry planes in the center of the geometry (depth and width). Here ① indicates the iso-surface of the liquidus temperature of the casted alloy $T_{liquidus}$ = 1259 K, ② the volume fraction solid f_c = 0.5 and ③ the iso-surface of f_c = 0.9. These three iso-surfaces are also displayed in the following figures. The zoomed picture in Figure 8b shows the relative velocity field between liquid and solid in the mushy zone. It can be seen that the density difference between liquid and solid causes feeding flow in the musy zone to move towards the wall of the strand. Figure 9 and Figure 10 show the calculated liquid and solid concentration of Sn and P in the marked region in Figure 8a. It can be seen that due to the different solubility the solid concentration is much lower than that of the liquid.

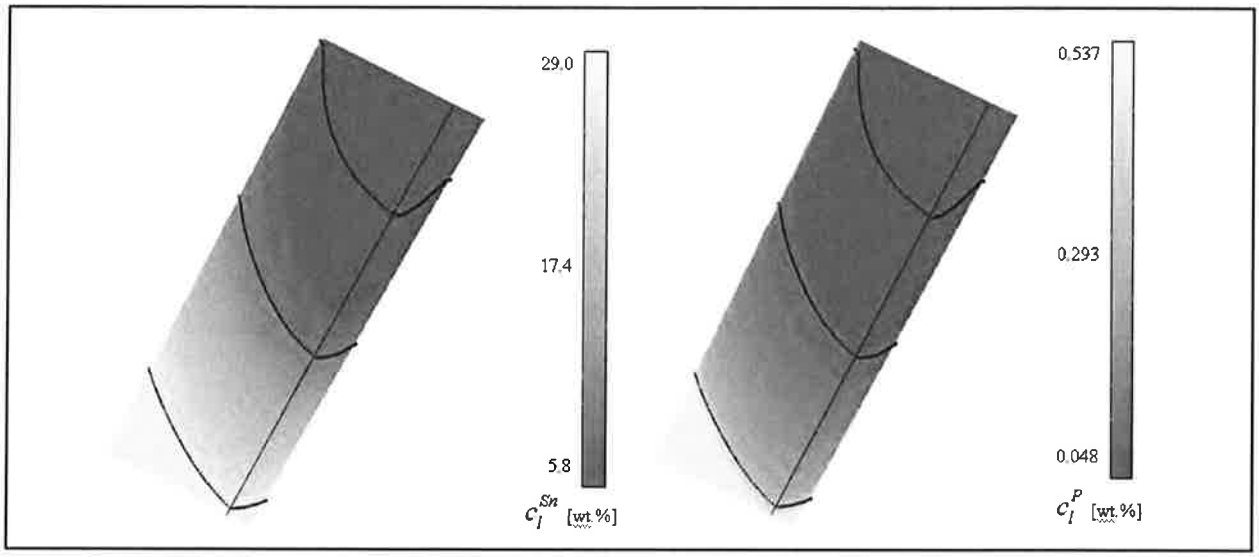

Figure 9: Calculated liquid concentration c_l^i (i = Sn, P) in the region marked with the rectangle in Figure 8a for the alloy CuSn0.58P0.048.

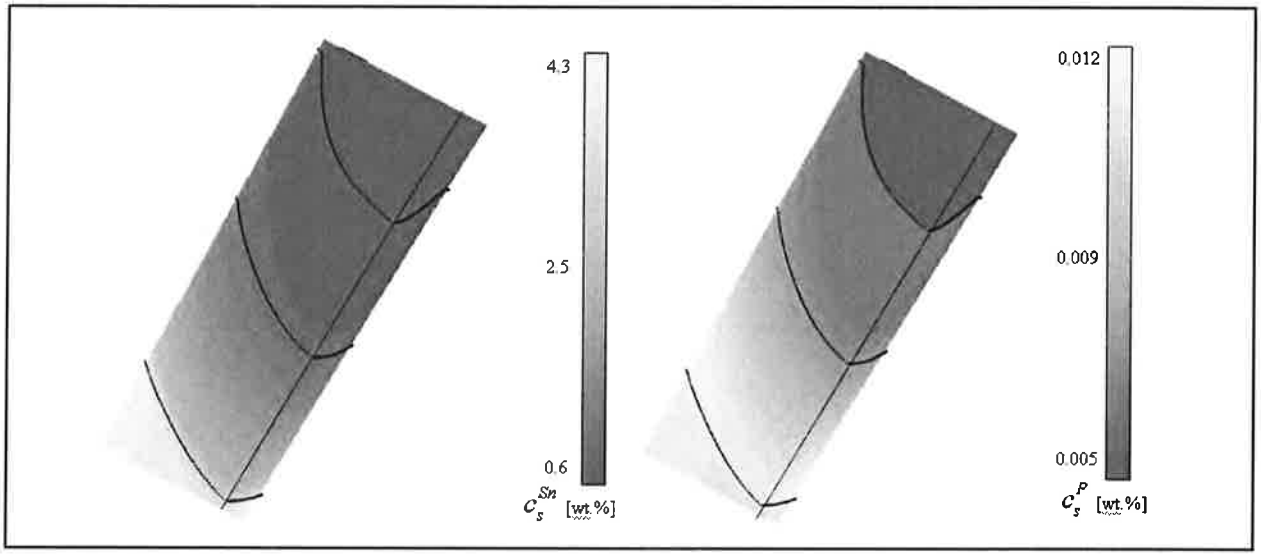

Figure 10: Calculated solid concentration c_s^i (i = Sn, P) in the region marked with the rectangle in Figure 8a for the alloy CuSn0.58P0.048.

In Figure 11 the predicted liquid concentrations for Sn and P are shown in comparison with a ternary Scheil calculation done with Thermo-Calc. The curves were taken in casting direction along the lines at the symmetry plane labelled in Figure11a. It can be seen that the calculated liquid concentrations are in agreement with the Scheil curve. However, it should be noted that the f_l versus c_l^{Sn} and c_l^{P} curves are slightly shifted compared to the ternary Scheil curves. One reason for that is Scheil does not consider any influence of the flow field on the concentration distribution but in our simulation forced convection and feeding flow are included. In addition, in the Scheil approach diffusion is thought to be infinitely high whereas in the simulation a diffusion coefficient of 10^6 is applied to the liquid. The zoomed pictures in Figure 11b and Figure 11c show that the position of the

profile in the strand also makes a difference. This is caused by the fact that there are different flow conditions in the casting. That means that in the centre, where we observe strong feeding flow and with that a depletion of Sn and P, the liquid concentrations are shifted to higher volume fractions solid whereas at the surface, where the solute is accumulated, the liquid concentrations are shifted to lower volume fractions.

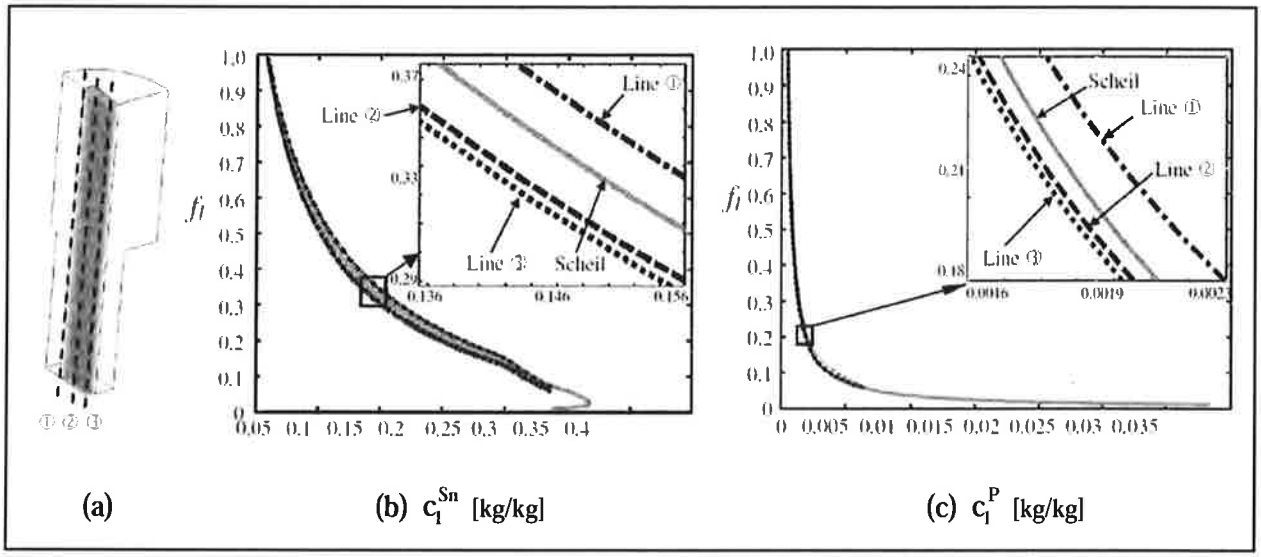

Figure 11: Scheil curve calculated with Thermo-Calc (gray line) for (b) Sn and (c) P compared to the f_l as function of c_l^{Sn} and c_l^{P} calculated for CuSn5.8P0.048 along three lines on the symmetry plane labelled in (a).

In order to study macrosegregation quantitatively a mixture concentration c_{mix}^i is defined according to [15]

$$c_{mix}^i = \frac{c_l^i \; _l f_l + c_c^i \; _c f_c}{_l f_l + \; _c f_c} \text{ , where i = Sn, P} \qquad (3)$$

Here, c_c^i is the cumulative solid concentration corresponding to the shell wise growth during solidification, c_l^i the corresponding concentration in the liquid, f_l and f_c volume fraction of liquid and columnar solid phase and $_l$ and $_c$ the corresponding densities.

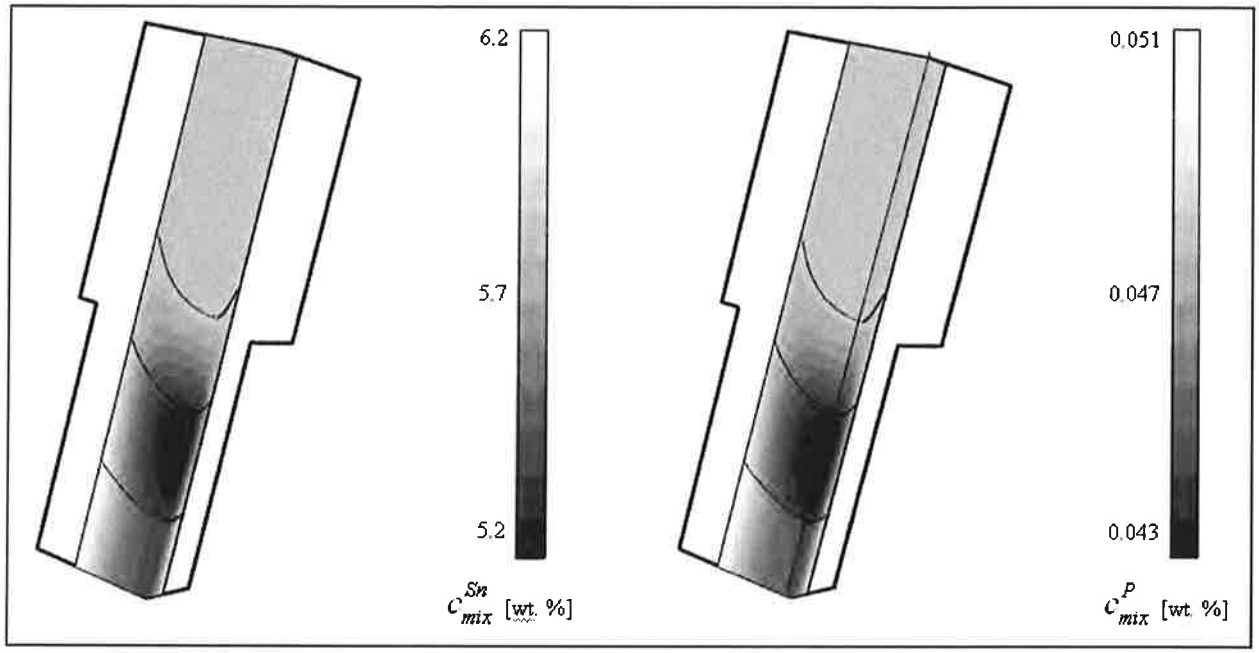

Figure 12: Macrosegregation c^{i}_{mix} (i = Sn , P) calculated with the two-phase volume averaging simulation for CuSn5.8P0.048.

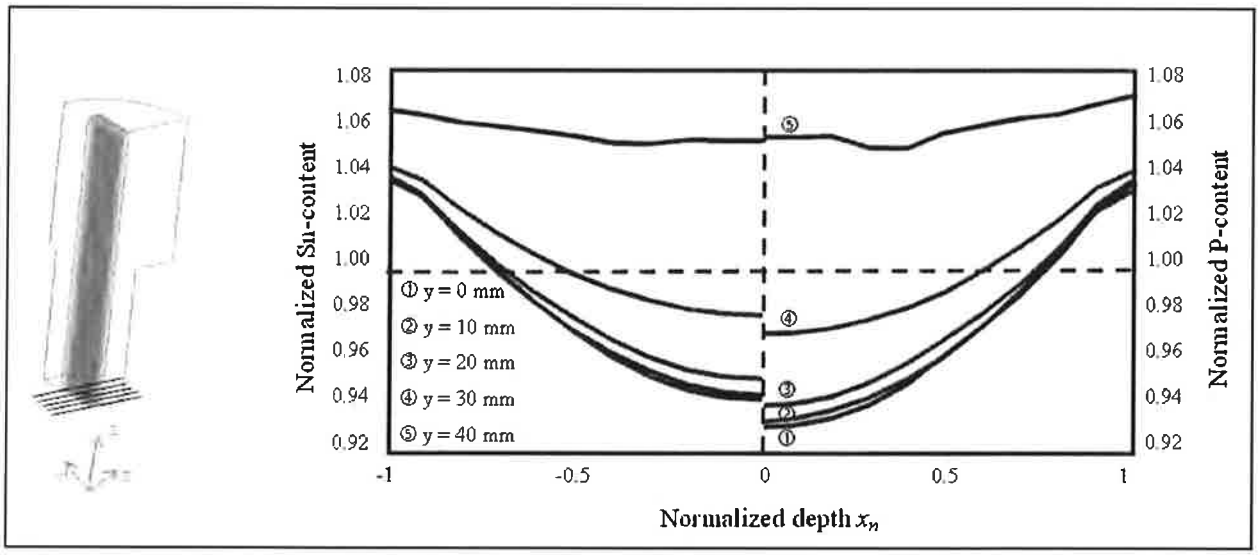

Figure 13: Calculated macrosegregation profiles of Sn (left) and P (right) along the depth at the outlet plane for y = 0 mm to y = 40 mm.

In Figure 12 the c^{Sn}_{mix} - and c^{P}_{mix} - distribution at the two symmetry planes are shown as calculated. Gray color shows the initial alloy concentration, black positive and white negative macrosegregation in the strand. Figure 13 shows some profiles taken along the casting cross section to display the concentration change within one plane close to the outlet which corresponds to the concentration distribution observed in the solidified casting. The predicted macrosegregation distribution shows the same tendency as observed in the experimental work (see Figure 3) namely, positive macrosegregation occurring at the surface and negative one in the centre of the casting. However, at the

moment the predicted values are not quantitatively comparable with the experimental results. One reason for that could be that we stop the mass transfer and with that the solute transfer between liquid and solid at a certain concentration. In addition, just feeding flow was considered in the simulation but thermo-solutal convection was ignored up to now. Therefore, in future the model has to be improved to include the eutectic transformation and the influence of other flow phenomena should also be studied.

5 Summary

Macrosegregations in DC casting are caused by a relative motion between solid and liquid during the solidification process. Thermodynamic data is included into solidification simulation with the software FLUENT by using spline-interpolation techniques to model the liquidus surface and the solubility of Sn and P in the different phases. The presented model was applied to a laboratory continuous casting process.

Concluding the following is stated:

- Ternary simulation based on nonlinear splines of the third order to approximate T_L, $\tilde{c}_c^{Sn}$ and $\tilde{c}_c^{P}$ compared well with ternary Scheil calculations. Some deviations are observed due to the difference between the solidification model presented which is based on diffusion-controlled solidification kinetics and Scheil's model which assumes infinite diffusion in the liquid. The position of the profile in the strand also has an influence on the macrosegeregation, which is mainly caused by the different flow conditions in the casting.
- The predicted macrosegregation of Sn and P shows the same distribution pattern as observed in experimental investigations, namely positive at the wall and negative in the center of the strand. Up to now, quantitative agreement with the measurement was not fully obtained. One reason for that could be that the applied thermodynamic model is developed for modelling peritectic transformation in a ternary system but the eutectic transformation is not yet considered, and therefore the solidification has to be stopped at a certain point. Besides, just shrinkage induced feeding flow is applied in the presented model. Other flow phenomena may also influence the formation of macrosegregation.

Based on the liquid and solid concentration of the calculation microsegregation and macrosegregation can be predicted for the solidified strand. Further work should be performed to improve the model for the inclusion of the eutectic transformation and other convection phenomena.

Acknowledgement

This work was financially supported by the Austria Christian-Doppler Society (CDG) and Wieland Werke for which the authors kindly acknowledge.

References

[1] http://www.anchorbronze.com, 2007.

[2] KAUFMAN L., BERNSTEIN H.: Computer Calculation of Phase Diagrams with Special Reference to Refractory Metals, Academic Press, New York, 1970.

[3] ANDERSSON J.O., HELANDER T., HÖGLUND L., SHI P., SUNDMAN B.: Thermo-Calc and DICTRA, Calphad, 2002, 26, pp. 273-312.

[4] SUNDMAN B., JANSSON B., ANDERSSON J.O.: The Thermo-Calc Databank System, Calphad, 1985, 9, pp. 153-169.

[5] JIE W.Q., ZHANG R., HE Z.,: Thermodynamic Description of Multi-Component Multi-Phase Alloys and Its Application to the Solidification Process, Mater. Sci. Eng. A. 2005, 413-414, pp. 497-503.

[6] KRAFT T., RETTENMAYR M., EXNER H.E.: Modeling of Dendritic Solidification for Optimizing Casting and Microstructure Parameters, Progress in Mater. Sci., 1997, 42, pp. 277-286.

[7] LAROUCHE D.: Computation of Solidification Paths in Multiphase Alloys with Back-Diffusion, Calphad, 2007, 31, pp. 490-504.

[8] ESKIN D. G., DU Q., NADELLA R., TURCHIN A.N., KAGERMAN L.: Reprogrammable FPLA with Universal Test Set, Proc. of the 5th Dec. Int. Conf. on Solid. Proc., 2007, pp. 437-441.

[9] GRUBER-PRETZLER M., PhD Theses, University of Leoben, 2008.

[10] LUDWIG A., GRUBER-PRETZLER M., MAYER F., ISHMURZIN A., WU M.: A Way of Coupling Ternary Phase Diagram Information with Multiphase Solidification Simulations, Mat. Sci. Eng. A, 2005, 413-414, pp. 485-489.

[11] LUDWIG A., ISHMURZIN A., GRUBER-PRETZLER M., MAYER F., WU M.: Combining Ternary Phase Diagram Information with Multiphase Solidification Simulations, Proc. of the 5th Dec. Int. Conf. on Solid. Proc., 2007, pp. 493-496.

[12] ISHMURZIN A., GRUBER-PRETZLER MAYER M., F., KÖNÖZSY L., WU M., LUDWIG A.: Multiphase/Multicomponent Modeling of Solidification Processes: Coupling Solidification Kinetics with Thermodynamics, IJMR, 2008, 99, pp. 618-25.

[13] GRASSER M., ISHMURZIN A., MAYER F., WU M., LUDWIG A., HOFMANN U., RIEDLE J.: Micro-Macrosegregation Prediction Based on Solidification Simulation for Continuous Casting of Ternary Bronze Alloys, McWASP XII, 2009, pp. 221-228.

[14] LUDWIG A., WU M., Modeling of Globular Equiaxed Solidification with a Two-Phase Approach, Metall. Mater. Trans., 2002, 33A, pp. 3673-3683.

[15] WU M.: Habilitationsschrift, University of Leoben, 2007.

[16] WU M., LUDWIG A.: A 3-Phase Model for Mixed Columnar-Equiaxed Solidification, Metall. Mater. Trans., 2006, 37A, pp. 1613-1631.

[17] WU M., LUDWIG A.: Using a Three-Phase Deterministic Model for the Columnar-to-Equiaxed Transition (CET), Metall. Mater. Trans., 2007, 38A, pp. 1465-1475.

[18] EFFENBERG G., ILYENKO S.: Cu-P-Sn (Copper-Phosphorus-Tin). Non-Ferrous Metal Ternary Systems - Selected Soldering And Brazing Systems: Phase Diagrams, Crystallographic And Thermodynamic Data, Non-Ferrous Metal Systems Part 3, 2007, 11C3, pp. 355-367.